

## Effects of Machine-To-Machine Variability on the Tensile Behavior of L-PBF Ti-6Al-4V

Mikyle Paul<sup>1,2</sup>, Shaikha Shohuda Tuktuk<sup>1,2</sup>, Matthew T. Lowney<sup>3</sup>, Shuai Shao<sup>1,2</sup>, Nima Shamsaei<sup>1,2\*</sup>

<sup>1</sup> *Department of Mechanical Engineering, Auburn University, Auburn, AL 36849, USA*

<sup>2</sup> *National Centre for Additive Manufacturing Excellence (NCAME), Auburn University, Auburn, AL 36849, USA*

<sup>3</sup> *U.S. Army DEVCOM Ground Vehicles System Center (GVSC), Warren, MI 48092, USA*

\* Corresponding author:

Email: [shamsaei@auburn.edu](mailto:shamsaei@auburn.edu)

Tel: (334) 844 4839

### **Abstract**

As additive manufacturing (AM) techniques are more frequently adopted for the fabrication of parts in load bearing applications, the understanding of the reproducibility of parts is important for the acceptance of AM by industries. Similar machines having different serial numbers are expected to yield parts with the same mechanical properties, however, this may not be the case if machines have not been adequately qualified and maintained. This study aims to assess the effects of machine-to-machine variability on the tensile behavior of Ti-6Al-4V fabricated on two Velo 3D Sapphire laser powder bed fusion machines at different geographical locations. Results showed that tensile properties were comparable across both builds. The most noticeable differences were observed in the ductility of the material which showed some location dependence. The location dependence, however, was the same for both machines.

**Keywords:** Laser powder bed fusion (L-PBF/LB-PBF), Ti-6Al-4V, Equivalency, Microstructure, Tensile behavior

## **Introduction**

Additive manufacturing (AM) is a technique used to create three-dimensional objects by consolidating material layer-by-layer [1–8]. Laser powder bed fusion (L-PBF) is one of the more popular AM processes enabling fabrication of parts with high geometric complexity, near-net-shape production, consolidation of multiple components, and efficient material usage [4,9]. As such, L-PBF has gained popularity in various industries including aerospace, biomedical, and automotive [10,11]. Parts fabricated via L-PBF often have complex microstructures, process induced volumetric defects, and undesirable residual stresses which can be detrimental to mechanical performance [12–15]. Numerous process parameters are carefully controlled during fabrication to ensure reproducibility of parts, however, this becomes challenging due to the variation in thermal histories depending on part geometry and process variables depending on machine control systems. These challenges hinder further adoption of L-PBF by industries.

Machine-to-machine equivalency in AM is a topic that is gaining much interest as it aims to understand the differences, if any, in part quality on the same or different machines [16]. Equivalency can be categorized into three different sectors: 1) repeatability, 2) reproducibility, and 3) cross-equivalency. Repeatability assesses the production of parts several times on the same machine, i.e., multiple iterations of the same build. Reproducibility assesses the production of parts on identical machines with different serial numbers. Cross-equivalency assesses the production of parts on machines from different original equipment manufacturers (OEMs). Reproducibility is one of the sectors that most OEMs are aiming to lock down but is challenging due to the unique micro-/defect-structures induced during L-PBF. Although identical build files, materials, and process parameters can be used on the same machine type with different serial numbers, variations in machine control systems, key process variables, machine health, and maintenance can lead to differences in part quality [17]. Both OEMs and standardization organizations are working towards establishing consistent L-PBF process for a range of materials and developing qualification programs to ensure parts produced by L-PBF are of acceptable quality [18,19].

Some of the other considerations that affect part quality are part orientation, which is due to grain directionality along the build direction [20,21], and part location relative to the recoater and shielding gas inlet which can affect the defect population [22]. This is an important design factor to consider for materials that show differences in mechanical properties depending on microstructural orientation and process induced volumetric defect content such Ti-6Al-4V which is commonly used in industrial applications [23,24]. To expand on the understanding of reproducibility in L-PBF, this study aims to assess the tensile behavior of Ti-6Al-4V grade 23 parts fabricated on the same machine model but with different serial numbers and at different geographical locations. The effects of part orientation and location on the microstructure and tensile behavior of the material have been studied and compared.

## Experimental methods

Plasma atomized Ti-6Al-4V grade 23 powder supplied by Tekna was used as the feedstock in this study with a particle size distribution of 20 – 53  $\mu\text{m}$ . Two Velo3D Sapphire L-PBF systems were used for fabrication of all test material. One machine was located in Oklahoma, United States and the other in Tokyo, Japan. Each machine was equipped with two 1 kW lasers, each covering half the build platform. The Velo3D sapphire machine uses a circular build platform with a diameter of 315 mm and maximum build height of 400 mm. Prior to this study, each machine underwent a standard Velo3D qualification process for Ti-6Al-4V grade 23 powder to ensure that each machine was in good operating condition according to Velo3D specifications.

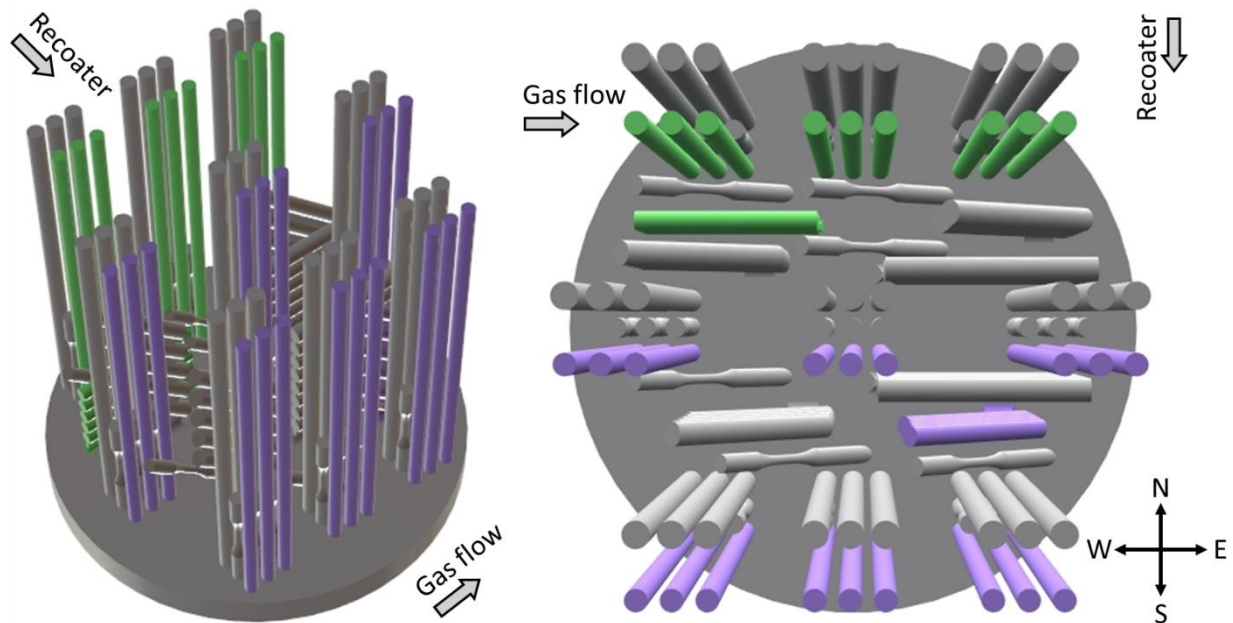


*Figure 1: Build layout used for fabrication of all test material on both Velo3D Sapphire machines.*

The build layout used in this study has been included in Figure 1. In order to prevent machine-to-machine variations, Velo3D utilizes a “Golden Print File” which contains identical process and machine parameters to ensure that whatever machine is used, parts of the same quality can be produced as long as the machines have been successfully qualified on the same feedstock. In Figure 1, various parts can be observed, however, only the colored ones have been used in this study with green and purple representing parts fabricated with Laser 1 and Laser 2, respectively. Cylindrical bars were fabricated in different forms to extract tensile specimens in various orientations including vertical, diagonal, and horizontal. The specimen extraction strategy and specimen geometry have been included in Figure 2. Additionally, for the vertical bars, part location on the build platform was taken into consideration by placing bars in nine different locations on the platform, i.e., north (N), south (S), east (E), west (W), center (C), northeast (NE), northwest (NW), southeast (SE), and southwest (SW). Here, N is towards the back of the machine and S is

towards the door of the machine. Although the vertical bars were fabricated to be 275 mm, only the bottom section was used for machining tensile specimens as depicted in Figure 2.

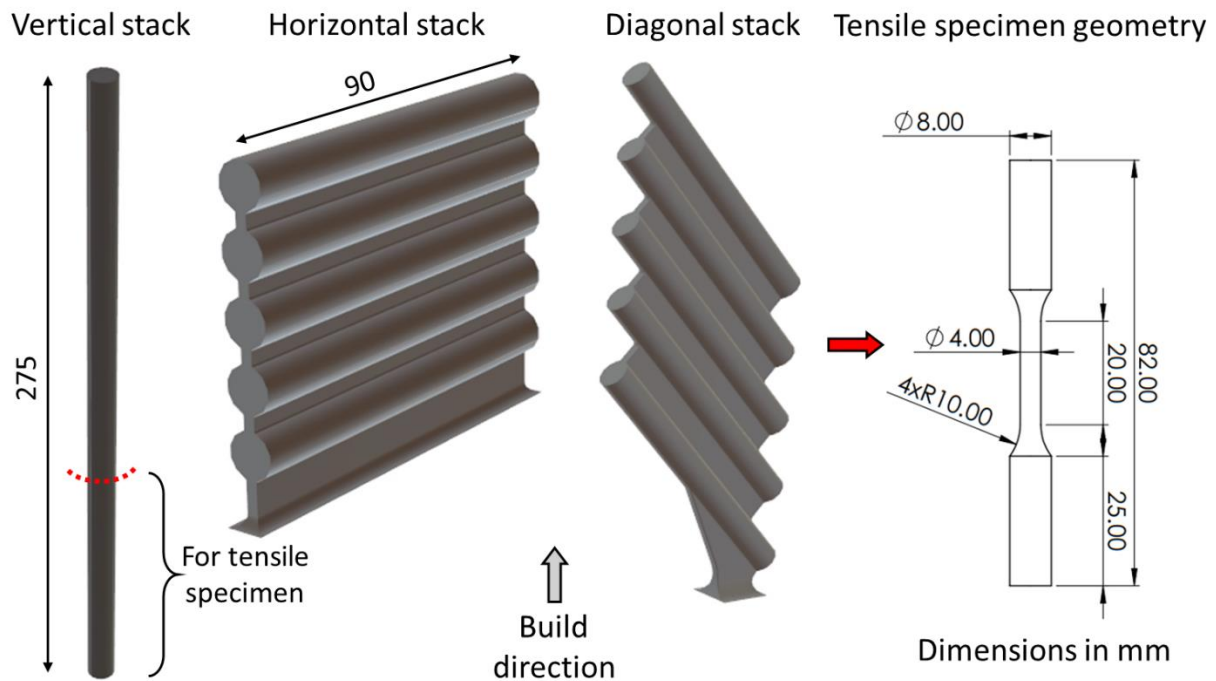


Figure 2: Tensile specimen extraction strategy and specimen geometry.

To save space on the build platform, horizontal and diagonal specimens were stacked, and the effects of part location were not considered for these orientations. After fabrication, both build platforms with parts still attached were stress relieved at 750 °C for 2 hours by external vendors in Oklahoma and Tokyo to relieve residual stresses induced during fabrication. The furnace was purged with argon gas to prevent oxidation during stress relief. Specimens were extracted from the platform using wire electrical discharge machining and turned down to the geometry specified in ASTM E8 [25].

Microstructural analysis was conducted on each orientation from each machine on coupons extracted from the grip section of tested tensile specimens on the plane parallel to the loading direction. Metallographic preparation of the coupons was conducted according to the guidelines in ASTM E3 [26]. Coupons were mounted in epoxy and ground using progressively finer grit sandpapers (from 280 to 1000 grit). Polishing was conducted using a ChemoMet polishing pad and 0.05  $\mu\text{m}$  colloidal silica to obtain a mirror finish. The mounted and polished coupons were then etched with Kroll's reagent for 20 seconds and the microstructure was observed with a Keyence VHX 6000 optical microscope.

Tensile tests were performed according to the procedures outlined in ASTM E8 on an MTS Landmark servo-hydraulic load frame equipped with a 100 kN load cell. The full test matrix has been included in Table 1. Initial loading was conducted at a strain rate of 0.005 mm/mm/min

controlled by an extensometer until a strain of 0.035 mm/mm was reached due to the limited range of the extensometer. Thereafter, the extensometer was removed, and the test was resumed in displacement control until fracture. Three specimens were tested per location for the vertical orientation whereas five specimens were tested each for the diagonal and horizontal orientations. The average yield strength (YS), ultimate tensile strength (UTS), elongation at failure (EL), area reduction (AR), and Young's modulus (E) per orientation and location were reported. A caliper was used to measure EL whereas optical imaging was used to measure AR. The fracture surfaces were analyzed after testing with a Zeiss Crossbeam 550 scanning electron microscope.

*Table 1: Test matrix for tensile testing.*

<b>Orientation</b>	<b>Number of Specimens</b>
Vertical	3 per location × 9 locations = 27
Diagonal	5
Horizontal	5

### **Results and discussion**

The microstructural results for each machine, denoted as Machine 1 and Machine 2, for each build orientation have been included in Figure 3. In all cases, typical microstructure for L-PBF Ti-6Al-4V can be observed which consist of prior  $\beta$  grains elongated in the build direction [27]. Within the prior  $\beta$  grains are colonies of  $\alpha$  laths. At temperatures above 995 °C ( $\beta$ -transus temperature), Ti-6Al-4V is purely in body centered cubic  $\beta$  phase which forms the initial structure of the material immediately after melting [28]. If the material cools slowly below the  $\beta$ -transus, hexagonally close packed  $\alpha$  phase nucleates and grows within the prior  $\beta$  grains. The size of the resulting  $\alpha$  colonies depends on the size of the prior  $\beta$  grains. Although grains are elongated in the build direction for each case, the difference exists in the loading direction relative to prior  $\beta$  grains. The major differences in microstructure are due to the build orientation rather than the machine.

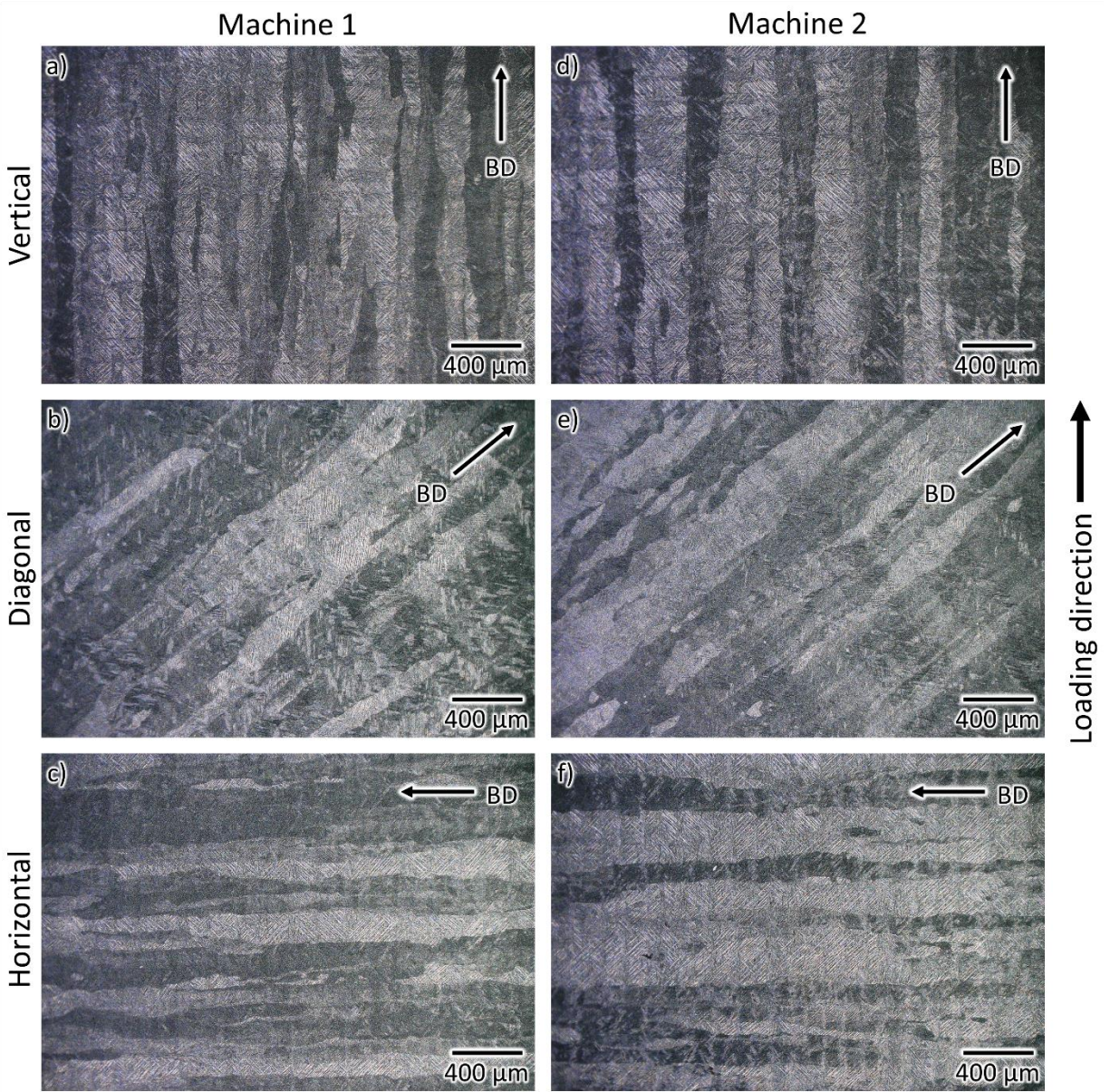


Figure 3: Microstructure of each orientation for a) Machine 1 and b) Machine 2.

The tensile test results for both machines have been included in Figure 4 with quantitative values included in Table 2. From Figure 4, it can be observed that the tensile properties of both machines are quite comparable for the same orientation. The major differences in properties arise from the difference in specimen orientation. In summary, the diagonal orientation exhibits the highest strength and lowest ductility whereas the vertical orientation exhibits the opposite trend.

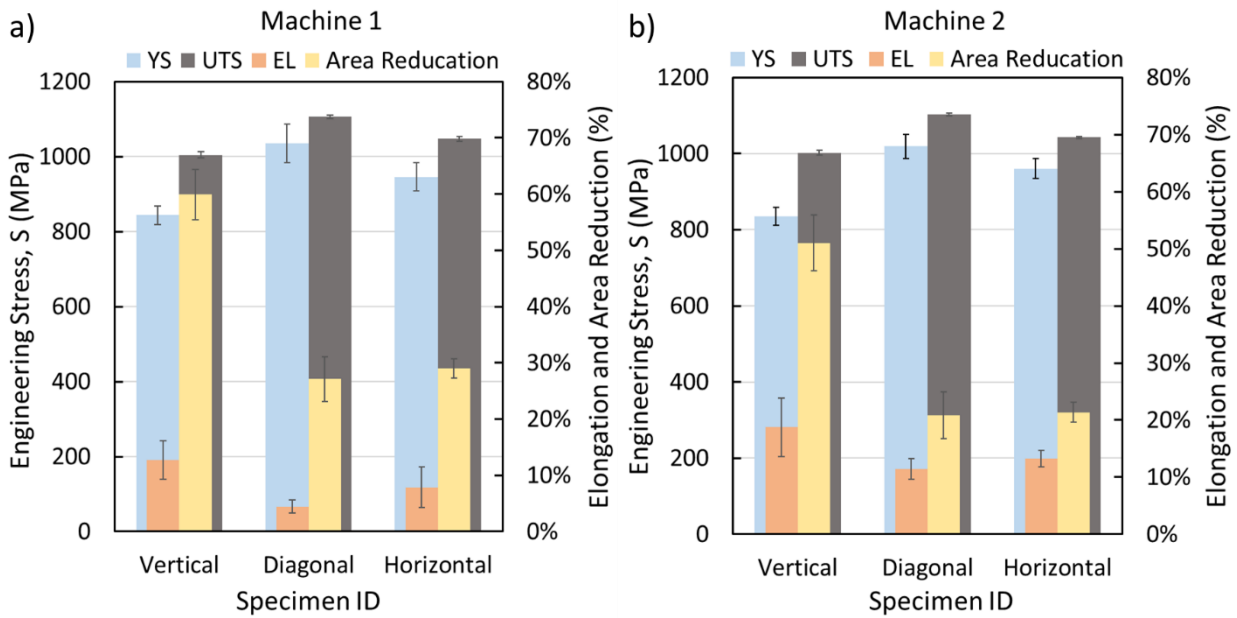


Figure 4: Summary of tensile test results for each machine.

Table 2: Quantitative summary of tensile test results for each machine and orientation.

Orientation	Machine	YS (MPa)	UTS (MPa)	EL (%)	AR (%)	E (GPa)
Vertical	1	844 ± 24	1005 ± 8	13 ± 3	60 ± 4	112 ± 0.8
	2	835 ± 23	1002 ± 6	19 ± 5	51 ± 5	112 ± 1.8
Diagonal	1	1035 ± 51	1106 ± 4	4 ± 1	27 ± 4	119 ± 1.0
	2	1019 ± 32	1103 ± 3	11 ± 2	21 ± 4	116 ± 2.1
Horizontal	1	946 ± 37	1047 ± 6	8 ± 4	29 ± 2	118 ± 0.7
	2	961 ± 26	1042 ± 3	13 ± 1	21 ± 2	115 ± 0.3

Comparing strength, i.e., YS and UTS (Figure 5a)), subtle differences can be observed between Machine 1 and Machine 2. The observed differences, however, are within the scatter bands included in the figure implying that they are not significant. YS and UTS are within the range of stress relieved L-PBF Ti-6Al-4V material in the literature for each orientation [27,29]. In Figure 5b), a clear separation in ductility measurements in terms of EL and AR can be observed between both machines. Machine 1 can be observed to show lower EL values and higher AR values compared to Machine 2 suggesting an earlier onset of necking in Machine 1 specimens. Ductility has been linked to process induced volumetric defect content in the literature [24] which could be a possible explanation as to why ductility differs among the two machines, however, defect content was not determined in this study.

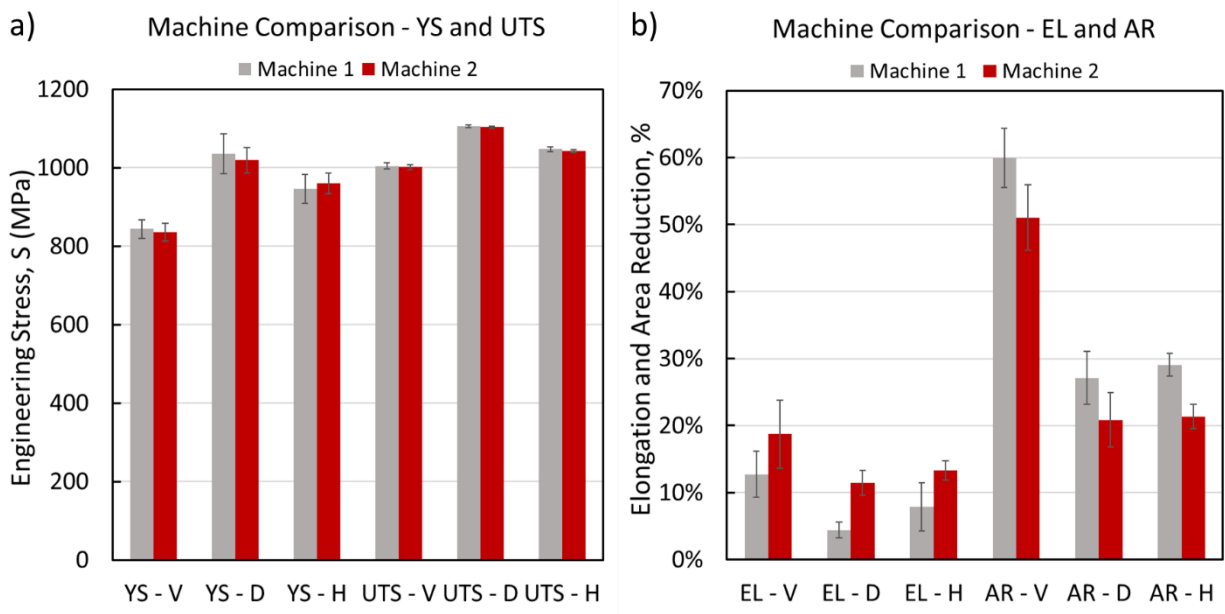


Figure 5: Side-by-side comparison of tensile properties for each machine.

To provide further insight into the fracture behavior, the fracture surfaces were analyzed (Figure 6). In the vertical specimens, a cup and cone fracture surface can be observed in both machines with significant AR compared to other orientations. Interestingly, large voids can be observed on the fracture surface of Machine 2 specimens which could have formed due to the growth of process induced volumetric defects resulting in the lower EL for Machine 2 vertical specimens. For diagonal and horizontal specimens, the cup and cone fracture surfaces cannot be observed and the resulting ductility in terms of both EL and AR can be observed to be less than in vertical specimens. For horizontal specimens, the shape of the fracture area can be observed to appear to be elliptical implying greater deformation in one direction. Step-like features can be observed on the fracture surface which appear to have aligned with the direction that underwent less reduction. These features could be due to the orientation of prior  $\beta$  grains which in the case of horizontal specimens were perpendicular to the loading direction [29].

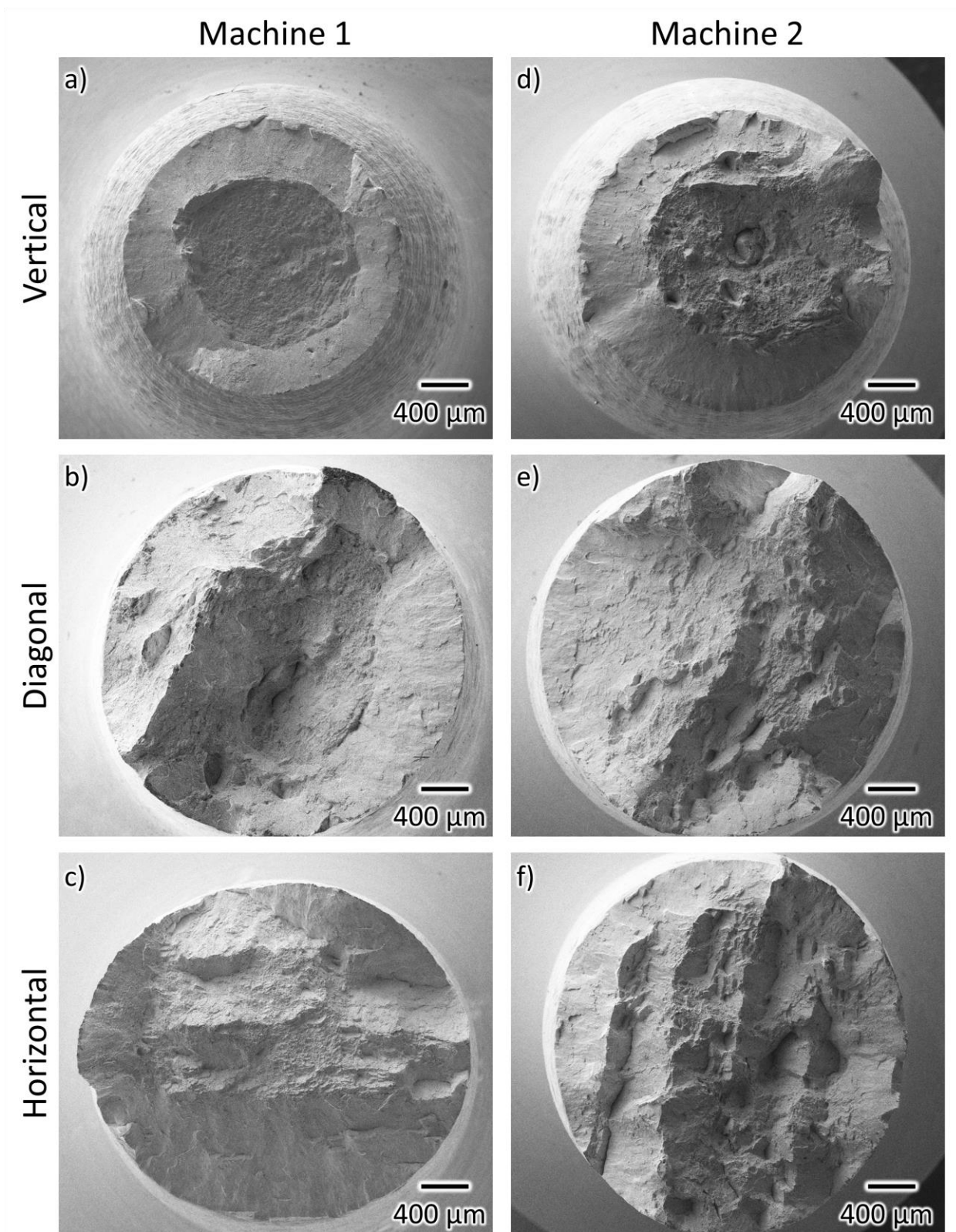


Figure 6: Fracture surfaces for different orientations in a) Machine 1 and b) Machine 2.

The effects of part location have also been investigated for the vertical orientation by fabricating specimens at nine different locations on the build platform. The tensile results have been reorganized based on location for both machines in Figure 7. In general, the UTS values for each location on each machine are consistent (approximately 1000 MPa) whereas YS shows subtle differences among locations. Considering ductility, some variations per location can be observed however, there is no correlation between location and gas flow or recoating direction. Since EL was measured using calipers, the observed differences may be due to minor measurement errors. Elongation at failure could not be captured with the extensometer due to its limited range. In general, Machine 2 exhibits more consistent strength and ductility measurements compared to Machine 1.

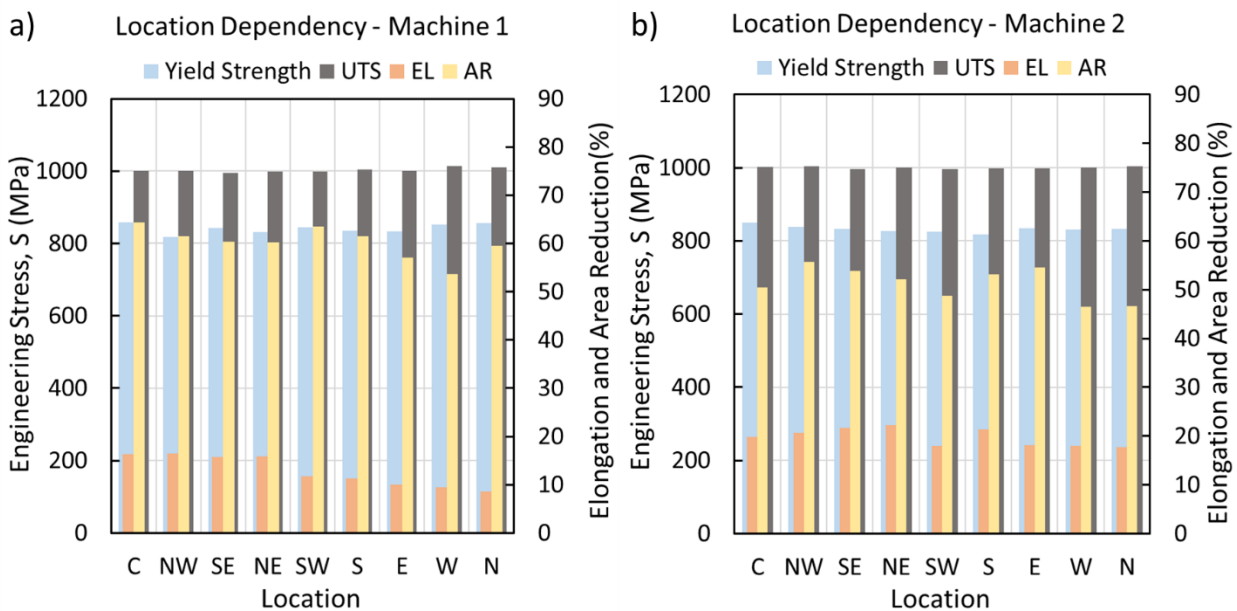


Figure 7: Location dependency in tensile properties for both machines.

Since each machine was equipped with a dual laser system, the differences in tensile properties between each laser have been included in Figure 8 to assess whether both lasers were operating according to specifications. According to the Velo3D slicing software, Laser 1 is assigned to the northern semicircle of the plate whereas Laser 2 is assigned to the southern semicircle. As depicted in Figure 1, the north specimens (green) were fabricated with Laser 1 and the south specimens as well as ones located near the middle line were fabricated with Laser 2. Tensile properties did not vary much with respect to laser assignment on each machine. Both machines had undergone the standard Velo3D material qualification processes which have been designed to capture any issues in laser operation performance therefore, the observed results were to be expected.

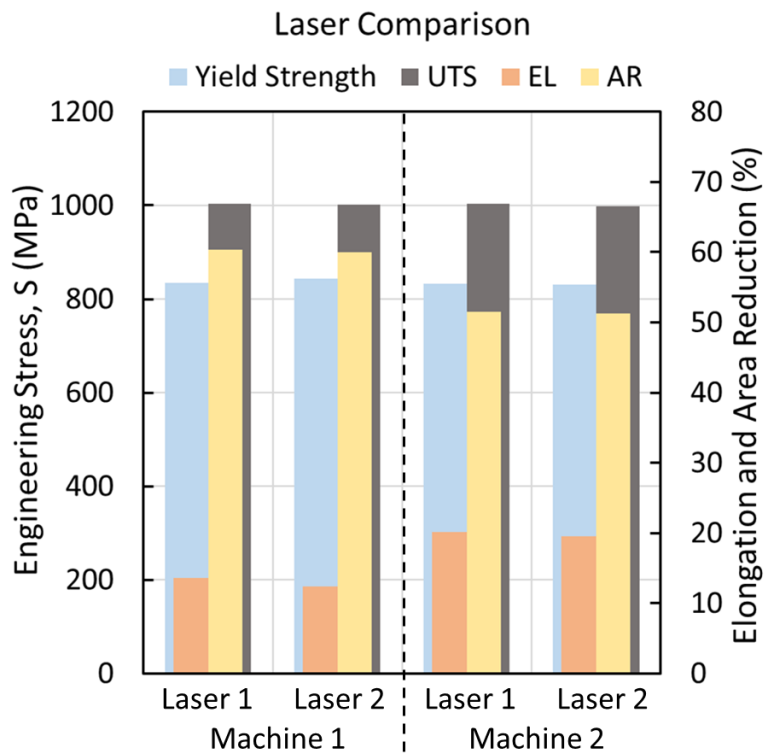


Figure 8: Comparison of tensile properties with respect to laser source for each machine.

### Conclusions

This study assessed the machine-to-machine equivalency through tensile behavior of Ti-6Al-4V grade 23 parts fabricated on power bed fusion machines of the same model but different serial numbers. The following conclusions can be drawn from the experimental results and analyses:

1. Differences in microstructure depended on specimen orientation rather than the machine used for fabrication.
2. Tensile strength was affected mainly by build orientation and subsequent grain orientation with vertical specimens exhibiting the lowest strength and diagonal specimens exhibiting the highest.
3. Ductility differed among orientations and machines likely due to the presence of process induced volumetric defects in the material.
4. There was little effect of part location on tensile properties for vertical specimens on each machine likely due to similar microstructures of vertical specimens resulting from similar thermal histories induced by identical part geometries.

## Acknowledgements

This research is based upon the work partially funded by the US Army Ground Vehicle Systems Center (GVSC) under grant No. UN-23-01810.

## References

- [1] W.E. Frazier, Metal Additive Manufacturing: A Review, *J Mater Eng Perform* 23 (2014) 1917–1928. <https://doi.org/10.1007/s11665-014-0958-z>.
- [2] B. Blakey-Milner, P. Gradl, G. Snedden, M. Brooks, J. Pitot, E. Lopez, M. Leary, F. Berto, A. du Plessis, Metal additive manufacturing in aerospace: A review, *Mater Des* 209 (2021) 110008. <https://doi.org/10.1016/j.matdes.2021.110008>.
- [3] N. Shamsaei, A. Yadollahi, L. Bian, S.M. Thompson, An overview of Direct Laser Deposition for additive manufacturing; Part II: Mechanical behavior, process parameter optimization and control, *Addit Manuf* 8 (2015) 12–35. <https://doi.org/10.1016/J.ADDMA.2015.07.002>.
- [4] S.L. Sing, W.Y. Yeong, Laser powder bed fusion for metal additive manufacturing: perspectives on recent developments, *Virtual Phys Prototyp* 15 (2020) 359–370. <https://doi.org/10.1080/17452759.2020.1779999>.
- [5] M. Paul, R. Ghiaasiaan, P. Gradl, J. Caron, P. Wang, S. Shao, N. Shamsaei, Tensile and fatigue behaviors of newly developed HAYNES® 233 alloy: Additively manufactured vs. wrought, *Mater Des* 244 (2024) 113165. <https://doi.org/10.1016/J.MATDES.2024.113165>.
- [6] E. Maleki, B. Salehnasab, M. Paul, S. Shao, N. Shamsaei, Dimensional accuracy of fabricated geometries through powder bed fusion: An overview and a new benchmark artifact proposal, *Mater Des* 257 (2025) 114361. <https://doi.org/10.1016/J.MATDES.2025.114361>.
- [7] I. Nandi, J. Welsh, J. Simsiriwong, S. Shao, N. Shamsaei, Fatigue strength prediction through defects-based analysis of L-PBF 17-4 PH stainless steel, (2022). <https://doi.org/http://dx.doi.org/10.26153/tsw/44169>.
- [8] S. Lee, Z. Ahmadi, M. Paul, M. Mahjouri-Samani, S. Shao, N. Shamsaei, In-situ tension investigation of additively manufactured silver lines on flexible substrates, *Additive Manufacturing Letters* 7 (2023) 100171. <https://doi.org/10.1016/J.ADDLET.2023.100171>.
- [9] I. Yadroitsev, A. Du Plessis, I. Yadroitsava, Basics of laser powder bed fusion, *Fundamentals of Laser Powder Bed Fusion of Metals* (2021) 15–38. <https://doi.org/10.1016/B978-0-12-824090-8.00024-X>.
- [10] R. Singh, A. Gupta, O. Tripathi, S. Srivastava, B. Singh, A. Awasthi, S.K. Rajput, P. Sonia, P. Singhal, K.K. Saxena, Powder bed fusion process in additive manufacturing: An

- overview, *Mater Today Proc* 26 (2020) 3058–3070. <https://doi.org/10.1016/J.MATPR.2020.02.635>.
- [11] D. Dev Singh, T. Mahender, A. Raji Reddy, Powder bed fusion process: A brief review, *Mater Today Proc* 46 (2021) 350–355. <https://doi.org/10.1016/J.MATPR.2020.08.415>.
- [12] P.J. Wilson, E. Azizian-Farsani, M. Paul, M.M. Khonsari, S. Shao, N. Shamsaei, On the damping and fatigue characterization of additively manufactured Ti-6Al-4V, *Additive Manufacturing Letters* 11 (2024) 100260. <https://doi.org/10.1016/j.addlet.2024.100260>.
- [13] P. Mercelis, J.P. Kruth, Residual stresses in selective laser sintering and selective laser melting, *Rapid Prototyp J* 12 (2006) 254–265. <https://doi.org/10.1108/13552540610707013>.
- [14] W. Sun, Y.E. Ma, P. Li, Z. Wang, Residual stress and long fatigue crack growth behaviour of laser powder bed fused Ti6Al4V: Role of build direction, *Int J Fatigue* 160 (2022) 106850. <https://doi.org/10.1016/J.IJFATIGUE.2022.106850>.
- [15] H. Gong, K. Rafi, T. Starr, B. Stucker, Effect of Defects on Fatigue Tests of As-Build Ti-6Al-4V Parts Fabricated by Selective Laser Melting, (2012). <https://doi.org/10.26153/TSW/15369>.
- [16] F. Uriati, G. Nicoletto, A comparison of Inconel 718 obtained with three L-PBF production systems in terms of process parameters, as-built surface quality, and fatigue performance, *Int J Fatigue* 162 (2022) 107004. <https://doi.org/10.1016/J.IJFATIGUE.2022.107004>.
- [17] M.S. Yasin, K. Stonaker, S. Shao, N. Shamsaei, Mechanical performance of laser powder bed fused Ti-6Al-4V: The influence of filter condition and part location, *Additive Manufacturing Letters* 11 (2024) 100255. <https://doi.org/10.1016/J.ADDLET.2024.100255>.
- [18] ASTM International, Additive Manufacturing-Process Characteristics and Performance: Practice for Metal Powder Bed Fusion Process to Meet Critical Applications, n.d. <http://www.ansi.org>.
- [19] ASTM International, Additive manufacturing-Qualification principles-Installation, operation and performance (IQ/OQ/PQ) of PBF-LB equipment, n.d. <https://www.iso.org/obp>.
- [20] M. Paul, S. Soman, S. Shao, N. Shamsaei, Fatigue crack growth in L-PBF Ti-6Al-4V: Influence of notch orientation, stress ratio, and volumetric defects, *Int J Fatigue* 198 (2025) 109027. <https://doi.org/10.1016/J.IJFATIGUE.2025.109027>.
- [21] V. Cain, L. Thijs, J. Van Humbeeck, B. Van Hooreweder, R. Knutsen, Crack propagation and fracture toughness of Ti6Al4V alloy produced by selective laser melting, *Addit Manuf* 5 (2015) 68–76. <https://doi.org/10.1016/j.addma.2014.12.006>.

- [22] A. Mussatto, R. Groarke, R.K. Vijayaraghavan, C. Hughes, M.A. Obeidi, M.N. Doğu, M.A. Yalçın, P.J. McNally, Y. Delaure, D. Brabazon, Assessing dependency of part properties on the printing location in laser-powder bed fusion metal additive manufacturing, *Mater Today Commun* 30 (2022) 103209. <https://doi.org/10.1016/J.MTCOMM.2022.103209>.
- [23] M. Benedetti, V. Fontanari, M. Bandini, F. Zanini, S. Carmignato, Low- and high-cycle fatigue resistance of Ti-6Al-4V ELI additively manufactured via selective laser melting: Mean stress and defect sensitivity, *Int J Fatigue* 107 (2018) 96–109. <https://doi.org/10.1016/J.IJFATIGUE.2017.10.021>.
- [24] M. Muhammad, M.S. Yasin, S. Soman, S. Shao, N. Shamsaei, Defect features critical to the fatigue of additively manufactured Ti-6Al-4V, *Theoretical and Applied Fracture Mechanics* 138 (2025) 104981. <https://doi.org/10.1016/j.tafmec.2025.104981>.
- [25] ASTM E8/E8M, Standard Test Method for Tension Testing of Metallic Materials, American Society for Testing and Materials (2013) 1–28.
- [26] ASTM, Standard Guide for Preparation of Metallographic Specimens Standard Guide for Preparation of Metallographic Specimens, ASTM International 03.01 (2012) 1–12.
- [27] M. Simonelli, Y.Y. Tse, C. Tuck, Effect of the build orientation on the mechanical properties and fracture modes of SLM Ti-6Al-4V, *Materials Science and Engineering A* 616 (2014) 1–11. <https://doi.org/10.1016/j.msea.2014.07.086>.
- [28] J.W. Pegues, S. Shao, N. Shamsaei, N. Sanaei, A. Fatemi, D.H. Warner, P. Li, N. Phan, Fatigue of additive manufactured Ti-6Al-4V, Part I: The effects of powder feedstock, manufacturing, and post-process conditions on the resulting microstructure and defects, *Int J Fatigue* 132 (2020) 105358. <https://doi.org/10.1016/j.ijfatigue.2019.105358>.
- [29] P.K. Singh, S. Kumar, P.K. Jain, U.S. Dixit, Effect of Build Orientation on Metallurgical and Mechanical Properties of Additively Manufactured Ti-6Al-4V Alloy, *J Mater Eng Perform* 33 (2024) 3476–3493. <https://doi.org/10.1007/s11665-023-08218-4>.